Pak. J. Bot., 58(2): 447-457, February 2026.

ARTICLE | DOI: http://dx.doi.org/10.30848/PJB2026-2(15)

PLANT-BASED SYNTHESIS OF ZNO NANOPARTICLES FROM *KALANCHOE PINNATA* LEAVES: A SUSTAINABLE APPROCH TO ANTIMICROBIAL NANOMEDICINE

SADIA SHERAZ[1], WALIULLAH KHAN[1*], KHUSHBAKHT ASAD[2], MANAL HADI GHAFFOORI KANAAN[3], MUHAMMAD SALMAN KHAN[2*], DILAWAR FARHAN SHAMS[4], ABDUR RAHIM[5], IKRAM ULLAH[6], FAROOQ AHMAD[2] AND FARHAD BADSHAH[7]

[1]Department of Chemistry, Abdul Wali Khan University Mardan, Mardan 23200, Pakistan
[2]Department of Botany, Abdul Wali Khan University Mardan, Mardan 23200, Pakistan
[3]Department of food industries, Technical Institute of Suwaria, Middle Technical University, Baghdad 10098, Iraq
[4]Department of Environmental Sciences, Abdul Wali Khan University, Mardan 23200, Pakistan
[5]Department of Zoology, University of Malakand, Chakdara, Dir Lower 18800, Pakistan
[6]School of Biological Sciences, Universiti Sains Malaysia, Penang 1180, Malaysia
[7]State Key Laboratory Biotech Breeding, Institute of Animal Science, Chinese Academy of Sciences, Beijing 100193, China

*Corresponding author's email: salman.khan@awkum.edu.pk; drwali@awkum.edu.pk

Abstract

Zinc oxide nanoparticles (ZnONPs) were successfully synthesized using *Kalanchoe pinnata, member of the family Crassulaceae,* leaf extract and zinc acetate as a precursor. This green synthesis method addresses the need for eco-friendly nanoparticle production and explores the potential of *K. pinnata*. UV–Vis analysis showed a surface plasmon resonance peak at 347 nm. FTIR confirmed the presence of biomolecules on the nanoparticle surface. SEM and particle size analysis revealed ZnONPs in the range of 50–120 nm, While EDX and XRD confirmed their elemental composition and crystalline structure, respectively. The synthesized ZnONPs exhibited strong antibacterial, antifungal, antioxidant, analgesic, anti-inflammatory, and antipyretic activities. Notably, they showed higher efficacy than plant extract alone, with the strongest antifungal effect against *Aspergillus niger* and antibacterial activity against *Escherichia coli*. These results suggest that *K. pinnata* mediated ZnONPs have significant biomedical potential. Future research should clarify the molecular mechanisms of *K. pinnata* mediated ZnONP synthesis, undertake comprehensive in vitro and in vivo toxicity studies, and optimize scalable production with stability assessments. Additionally, investigating controlled-release formulations and synergistic effects with standard therapeutics will enhance their potential for practical biomedical applications.

Key words: *Kalanchoe pinnata*; Zinc oxide; Nanoparticles; Biological applications; FTIR; XRD; SEM

Introduction

Nanotechnology is the design, synthesis and manipulation of materials sized 1-100 nm to exploit their unique physicochemical properties. In twenty-first century, nanotechnology has emerged as a multi-disciplinary area. Biosynthetic nanotechnology has applications in biomedical science, chemical industries, food or feed, cosmetics, healthcare, medicine and genetic factor delivery, mechanics, electronics, energy sciences and space. New physical and chemical characteristics are created, and the new material can find numerous applications in areas such as material science and biomedical applications due to miniaturization of the material (Sivasankarapillai *et al*., 2019).

Zinc oxide nanoparticles (ZnO NPs) have emerged as promising nanomaterials in pharmacology due to their unique physicochemical properties and biocompatibility. Their application in targeted cancer therapy is particularly noteworthy; ZnO NPs act as pH-responsive carriers that release therapeutic agents in the acidic tumor microenvironment, inducing cytotoxic effects through reactive oxygen species (ROS) generation. Functionalization with ligands such as folic acid enhances cellular uptake and specificity, minimizing systemic toxicity (Swidan *et al*., 2024; Subramaniam *et al*., 2022). Additionally, green-synthesized ZnO NPs exhibit broad-spectrum antimicrobial activity, antioxidant potential, and antidiabetic effects. Their ability to disrupt microbial membranes, modulate oxidative stress, and improve glucose metabolism supports their use in treating infections and metabolic disorders (Ajmal *et al*., 2024; Nkemzi *et al*., 2024; Yousaf, 2024). These multifunctional roles position ZnO NPs as valuable candidates for future therapeutic applications.

In addition to the various synthesis method of generated zinc oxide, there is a need to study its morphology that the properties of zinc oxide depend on the morphology of its nanostructures. Zinc sulphate heptahydrate and sodium hydroxide were employed as precursors to develop ZnO NPs. After characterization by XRD and SEM the manufactured samples were subsequently analyzed using EDS to determine their purity. In order to establish the relationship between the optical properties of ZnO and its morphology and crystallite size an analysis of ZnO nanostructures morphology size and optical property was made (Kumar *et al*., 2013). ZnONPs are a new class of inexpensive, low-toxicity nanomaterials that have drawn a

Received: 08-02-2025 | Revised: 06-08-2025 | Accepted: 16-08-2025 | Online: 24-10-2025

lot of interest in a variety of biomedical domains, such as drug delivery and bio-imaging applications, as well as activities pertaining to anticancer, antibacterial, antioxidant, anti-diabetic, and anti-inflammatory qualities (Jiang *et al*., 2018) Conversely, biological methods are facilitated by either microbes or plants. The biological method of preparing metal nanoparticles is incredibly cost-effective in terms of energy, reaction time, safety, ease of use, and product yield (Yedurkar *et al*., 2016).

Zinc oxide nanoparticles (ZnONPs) have been extensively employed in degradation of contaminants and antimicrobial processes. They have a good antimicrobial action against those spores that are tolerant of heat and increased pressure. The discovery of new applicability of ZnONPs in biomedical engineering; some of the new fields of application include using them for coating implants, for wound healing and tissue engineering, as well as in the engineering of cancer fighting procedures (Iqbal *et al*., 2019). Medicinal plants are traditionally used in folk medicine as natural remedies for the controlling and treatment of many lethal diseases. with therapeutic effects and play important role for the treatment of many disease (Shinwari *et al*., 2018; Anjum *et al*., 2019; Khan *et al*., 2019; Ovais *et al*., 2019; Jan *et al*., 2022; Khan *et al*., 2023). *K. pinnata* of *crassulaceae* family a popular succulent plant originated in Madagascar is also commonly known as Goethe plant, cathedral bells, miracle leaf, and life plant. It is one of the most common house plants in the tropic and sub-tropics. It is an evergreen succulent plant that has fleshy cylindrical stems are reddish in their young state, grows to about 1-metre-high and flowers for about nine out of the twelve months of the year (Al-Snafi *et al*., 2013). According to the preliminary phytochemical examination, this work aims to establish the herbal resources possessing few pharmacological potentials. Although plant-mediated synthesis of ZnO nanoparticles is well-studied, the phytochemical constituents of *K. pinnata* have not been thoroughly investigated for this purpose. The influence of its bioactive compounds on ZnONP synthesis, stability, and multifunctional bioactivities remains unclear, limiting the advancement of efficient green-synthesized ZnONPs for biomedical applications. *K. pinnata* mediated ZnO nanoparticles exhibit markedly enhanced analgesic and antifungal activities compared to those synthesized from other plant extracts, highlighting the unique role of *K. pinnata* phytochemicals in producing multifunctional, green-synthesized nanoparticles. The present study focused on the green synthesis of zinc oxide nanoparticles (ZnONPs) using *K. pinnata* leaf extract and zinc acetate as a precursor. The synthesized ZnONPs were characterized by UV–Vis spectroscopy, FTIR, SEM, EDX, and XRD. Their antibacterial, antifungal, antioxidant, analgesic, anti-inflammatory, and antipyretic activities were evaluated and compared with those of the crude plant extract.

Material and Methods

Collection of plant material: Leaves of *Kalanchoe pinnata* (Fig. 1) were obtained from Peshawar, Pakistan, in October 2021. They were washed with distilled water, cut into small pieces, and air-dried at 25–30°C. The dried material was ground into fine powder using an electric grinder and stored in sealed amber bottles to protect against light, moisture, and degradation (Das *et al*., 2010). Prof. Dr. Waheed Murad identified the plant, and a voucher specimen (No. 125367) was deposited in the Herbarium of Abdul Wali Khan University Mardan.

Preparation of plant extract: Plant extract was prepared by weighing 10g of powdered *K. pinatta* leaves and adding 100 ml of distal water into a beaker and heating mixture on a hot plate for 20-25 minutes.

Green synthesis of zinc oxide nanoparticles: A total of 2 mg of zinc oxide was dissolved in 50 mL of distilled water. The solution was mixed with plant extract in a 1:25 ratio and heated at ~455°C with continuous stirring for 2 hours. Change of color from light yellow to whitish indicated the formation of ZnONPs due to phytochemical-mediated reduction of zinc ions (Dipankar *et al*., 2012). The nanoparticles were separated by centrifugation at 4500 rpm for 25–30 minutes, washed three times with distilled water, and oven-dried at 100°C for 3 hours.

Physical characterization

UV-Vis spectrophotometry: The formation of zinc oxide nanoparticles (ZnONPs) was assessed through ultraviolet–visible (UV–Vis) spectroscopy using a UV-1602 double-beam spectrophotometer with a spectral resolution of 1 nm. Distilled water was used as a reference blank. The reaction mixtures were prepared with varying ratios of *K. pinnata* leaf extract to zinc precursor (1:1 to 1:6) to evaluate the influence of extract concentration on nanoparticle synthesis. Absorbance was recorded over a wavelength range of 300–800 nm, and the appearance of a distinct absorption band indicated successful formation of ZnONPs (Acay *et al*., 2019).

FTIR spectrophotometry: The synthesized ZnO nanoparticles were dried at 37°C using a vacuum dryer to eliminate residual moisture. For FT-IR analysis, the dried ZnONPs were finely ground and homogenized with potassium bromide (KBr), then compressed into pellets using a hydraulic press. Spectral analysis was performed using a PerkinElmer Spectrum One FT-IR spectrometer in the range of 4000–400 cm^{-1} with a resolution of 4 cm^{-1} (Acay *et al*., 2019).

X-Ray spectrophotometry: ZnONPs prepared from *K. pinattta* extract were analyzed with jeOL JDX 3532 X-ray diffractometers. The diffraction patterns of the bio fabricated nanoparticles were obtained with the help of a nickel monochromator. Cu-K radiation was utilized to filter the wave at tube voltage of 40KV and the current of 30mA. The size of the ZnONPs related to the Scherr's equation $D = K\lambda / (\beta 1/2\cos\theta)$, in which Scherr's constant K = 0.93 and β is the Full width half maximum. Bragg angle X-ray wavelength is denoted here by λ(=1,5406A0), the shearer K (0.89) andβ is the coefficient (Acay *et al*., 2019).

Scanning electron spectroscopy: ZnONPs synthesized from an extract from *K. pinatta* leaves was vacuum dried at a temperature of 350**°C**. To prepare the ZnONPs sample, a very small volume of the sample was placed on a carbon mounted SEM grid and allowed to dry for some time before being coated in ZnO using an auto fine coater (Spi-module

sputter coater). Sample were then characterized using a scanning electron microscope (FE-SEM (JSM-5910-JEOL) in order to determine morphological features (Mofolo *et al*., 2020).

Energy-dispersive X-ray: The elemental composition of zinc in the synthesized ZnO nanoparticles was confirmed using energy dispersive X-ray spectroscopy (EDS). The nanoparticle suspension was vacuum-dried at 35°C, following centrifugation at 4800 rpm for 15 minutes. The dried sample was then analyzed using an Oxford Inca 200 EDS system attached to a scanning electron microscope (SEM) (Mofolo *et al.,* 2020).

Biological assays

Anti-oxidant assay: Antioxidant activity of *K. pinnata* extract and ZnONPs was assessed using the DPPH assay. A 0.004% DPPH solution was prepared in 99.9% methanol. Test samples (plant extract, ZnONPs, and ascorbic acid) were prepared at 50, 100, and 500 µg/mL. Equal volumes of each sample were mixed with 2 mL of DPPH solution to make a final volume of 3 mL. The mixtures were kept in the dark at 25°C for 60 minutes. Absorbance was recorded at 517 nm using a UV–Vis spectrophotometer. Lower absorbance indicated higher antioxidant activity (Khan *et al.,* 2018).

$$\text{Antioxidant potential \%} = \frac{\text{Absorbance of control (nm)} - \text{Absorbance of sample (nm)}}{\text{Absorbance of control}} \times 100$$

Anti-fungal assay: Antifungal activity of *K. pinnata* extract and ZnONPs was tested using the agar well diffusion method. PDA medium (20 mL) was poured into sterile Petri dishes and incubated at room temperature for 24 hours to check for contamination. A 10 µL fungal suspension was spread on the solidified medium. Four wells of 5 mm each were made in each plate, and 50, 100, and 500 µL/mL of plant extract and ZnONPs were added. Clotrimazole and distilled water were used as positive and negative controls, respectively. Plates were incubated at 25°C for 3–7 days, and inhibition zones were measured after 72 hours to assess antifungal efficacy (Keshari *et al.*, 2020).

Antibacterial assay: The antibacterial activity of *K. pinnata* extract and ZnONPs was evaluated using the Kirby-Bauer disc diffusion method. All materials were autoclaved at 121°C and 17 lb pressure for 1 hour. A 10 µL bacterial suspension was spread on solidified agar medium using a sterile glass spreader. Four discs were placed on each plate, loaded with test samples at varying concentrations. Streptomycin and distilled water served as positive and negative controls, respectively. Plates were incubated at 25°C for 24 hours, and the diameter of inhibition zones was measured to assess antibacterial activity (Asad *et al.*, 2025a).

Analgesic activity: The analgesic potential of *K. pinnata* ethanolic leaf extract was assessed using the acetic acid-induced writhing test in Swiss albino mice, with ethical approval granted by the Abdul Wali Khan University Ethics Committee, Mardan, KPK, Pakistan. Mice were randomly divided into six groups. The control group received 1 mL of 1% saline intraperitoneally, while the second group (disease control) was given 1 mL of 1% acetic acid only. The remaining groups were injected with 1 mL of acetic acid followed by treatments: Group III received paracetamol, and Groups IV to VI received ethanolic leaf extract at concentrations of 50, 100, and 500 µL/mL, respectively. Writhing responses were observed for five minutes, beginning ten minutes after acetic acid administration. The reduction in the number of writhes was used to calculate the percentage inhibition, indicating the analgesic effect of the test substances (Asad *et al*., 2022; Asad *et al*., 2024).

$$\text{Inhibition (\%)} = \frac{\text{Number of writhing in sample group}}{\text{Number of writhing in the control group}} \times 100$$

Anti-inflammatory assay: Male Swiss albino mice (25–30 g) were selected for the study and housed individually in clean plastic cages under controlled conditions (20–25°C, 50–60% humidity), where they were regularly provided food and water. The animals were habituated for ten days under standard laboratory conditions. Prior to testing, mice were fasted overnight, and experiments were conducted between 8:00 AM and 12:00 PM. Ear inflammation was induced by applying two drops of xylene to one ear of each mouse, and ear thickness was measured 15–20 minutes later to confirm edema. Treatment groups received *K. pinnata* ethanolic extract topically at concentrations of 50, 100, and 500 µL/mL using micropipettes, while the standard group was treated with 10 µg/ear of diclofenac sodium. The positive control group did not receive xylene. This protocol was used to evaluate the anti-inflammatory potential of the plant extract (Liu *et al*., 2020; Asad *et al*., 2024).

$$\text{\% Inhibition ear edema} = \frac{\text{(Thickness of control} - \text{Thickness of the treated)}}{\text{Thickness of the control group}} \times 100$$

Anti-pyretic assay: The *In vivo* antipyretic activity was evaluated using a Brewer's yeast-induced pyrexia model in male Swiss albino mice. Fever was induced by subcutaneous injection of a 10% w/v Brewer's yeast suspension at a dose of 10 mL/kg. Prior to yeast administration, the baseline rectal temperature of each mouse was recorded using a lubricated digital thermometer. After 18 hours, a second temperature reading was taken to confirm the onset of pyrexia. The mice were then administered the test substances intraperitoneally. Rectal temperatures were monitored at hourly intervals for a total duration of four hours to assess the antipyretic response (Sulaiman *et al*., 2022; Asad *et al*., 2024).

Statistical analysis

Data (n = 6) were analyzed using one-way ANOVA followed by Dunnett's test in SPSS v16.0. Graphs were prepared using OriginPro 7.5.

Fig. 1. *Kalanchoe pinatta* plant.

Results and Discussion

UV spectrophotometry: The formation of ZnO nanoparticles was confirmed using a dual-beam UV–Vis spectrophotometer. Absorption spectra recorded between 200–600 nm (Fig. 2) showed a distinct peak at 347 nm for ZnO NPs synthesized with *Kalanchoe pinnata* extract. This peak indicates surface plasmon resonance (SPR), confirming the presence and optical activity of the nanoparticles. Previous studies have reported UV–Vis absorption peaks characteristic of ZnO nanoparticles within the UV range. Yedurkar *et al*., (2016) observed maximum absorbance at 340 nm, while Mahmood *et al*., (2022) reported a prominent peak at 375 nm, both confirming successful synthesis of ZnO NPs. The ability of ZnO to absorb UV light is crucial for its photocatalytic activity, as it facilitates the excitation of electrons necessary for the photocatalytic process. Rajeshkumar *et al*., (2018) also confirmed the formation of ZnO NPs by a characteristic absorption peak at 355 nm following 6 hours of incubation. Similarly, Vijayakumar *et al*., (2015) demonstrated that green synthesis using *Plectranthus amboinicus* leaf extract yielded ZnO NPs with comparable UV absorption behavior. These findings support the current results, indicating effective synthesis and strong UV absorption capabilities of ZnO NPs.

FTIR Spectroscopy: Fourier-transform infrared (FTIR) spectroscopy was utilized to determine the functional groups involved in the reduction, capping, and stabilization of ZnO nanoparticles synthesized using *K. pinnata* leaf extract. The FTIR spectrum (Fig. 3) exhibited a broad band at 3277 cm^{-1}, which corresponds to O–H stretching vibrations and suggests the presence of hydroxyl groups. Additional characteristic peaks included 1558 cm^{-1} (indicative of C=C stretching), 1405 cm^{-1} (assigned to the C–N stretching vibration of amide I in proteins), 1027 cm^{-1} (attributable to C–O stretching in amino acids), 948 cm^{-1} (corresponding to C–O–C stretching vibrations), and bands at 677 cm^{-1} and 618 cm^{-1} (associated with C–H bending vibrations). Importantly, the spectrum also showed a distinct peak at 498 cm^{-1}, confirming the presence of Zn–O bonds and thereby validating the formation of ZnO nanoparticles. These results indicate that multiple phytochemicals present in the leaf extract are actively involved in the bioreduction and stabilization processes of the nanoparticles. A broad absorption band around 3398 cm^{-1} corresponded to O–H stretching, indicating the presence of hydroxyl groups. The peak observed at 533 cm^{-1} was attributed to Zn–O stretching vibrations, confirming the formation of ZnO nanoparticles. These observations were in agreement with those reported by Rao *et al*., (2015). Similarly, Awwad & Amer (2020) identified functional groups at 3505 cm^{-1} (O–H stretching), 1560 cm^{-1} (C=C aromatic), 1507 cm^{-1}, 1388 cm^{-1} (C–H bending), 1034 cm^{-1} (C–N stretching of aliphatic amines), and 885 cm^{-1} (aromatic C–H bending). The presence of similar functional groups in both the plant extract and the synthesized ZnO NPs suggests that phytochemicals from the extract play a significant role in reducing and stabilizing the nanoparticles.

X-rays diffraction analysis: The crystalline nature of the synthesized ZnO nanoparticles was confirmed by X-ray diffraction (XRD) analysis. Prominent diffraction peaks were observed at 2θ values of 30.55°, 36.2°, 48.3°, 56.45°, 63.4°, and 68.45°, corresponding to the (100), (101), (102), (110), (103), and (112) planes of ZnO, as shown in (Fig. 4). The sharp and well-defined peaks indicate a high degree of crystallinity. Crystallite size was estimated using the Scherrer equation: $D = 0.9\lambda / \beta cos\theta$. Additional peaks observed at 31.84°, 34.52°, 36.38°, 47.64°, 56.7°, 63.06°, and 68° further confirmed the crystalline structure. According to JCPDS card No. 36-1451, these reflections are characteristic of the hexagonal wurtzite shape of ZnO. The absence of extraneous peaks confirms the purity of the synthesized ZnO nanopowder, with no detectable secondary phases or impurities. Golmohammadi *et al*., (2020) reported the synthesis of spherical ZnO NPs ranging from 21–37 nm using *Ziziphus jujube* fruit extract. Similarly, Padalia & Chanda (2017) achieved spherical ZnO nanoparticles with sizes between 12.47–26.97 nm using *Ziziphus nummularia* leaf extract. According to Chemingui *et al*., (2019), during the green synthesis process, Zn^{2+} ions interact with electron-donating biomolecules present in the plant extract, leading to their reduction. Under alkaline conditions, $Zn(OH)_4^{2-}$ are initially formed, which then complex with phytochemicals such as polyphenols and flavonoids. Upon calcination $Zn(OH)_4^{2-}$ breaks down, resulting in the formation of pure ZnO nanoparticles. These findings align with the current study and reinforce the role of plant-based compounds in controlling particle morphology and aiding nanoparticle stabilization.

Scanning Electron Microscopy: Scanning electron microscopy (SEM) was used to analyze the surface morphology and particle size of the green-synthesized

ZnO nanoparticles (Fig. 5). The estimated crystallite size, calculated using the Scherrer equation, ranged between 50–120 nm. SEM images revealed that the nanoparticles primarily exhibited spherical to hexagonal shapes. The morphology was influenced by various synthetic conditions, including the precursor-to-extract ratio, stirring duration, and the activity of biofunctional groups. These factors likely played a key role in particle growth, aggregation, and shape variation during synthesis. Variations in the morphology and size of ZnO nanoparticles synthesized through green methods have been widely documented. Nazir *et al*., (2021) reported that ZnO nanoparticles with irregular, platelet-like structures, often formed aggregates due to surface interactions with stabilizing biomolecules present in the plant extract. Elemental analysis of their sample revealed high purity, with zinc and oxygen content recorded at 19.87% and 74.95%, respectively. In another study, Chikkanna *et al.*, (2019) described nanoparticles exhibiting spherical, flower-like, and sponge-like shapes, with particle sizes ranging from 40–120 nm for one formulation and 60–130 nm for another. Agarwal *et al*., (2017) also observed agglomeration among ZnO nanoparticles, contributing to slightly increased particle dimensions-an effect commonly seen in biosynthetic processes. Krupa *et al*., (2016) estimated an average particle size of 60 nm, which aligned with results from coconut water-mediated synthesis that produced particles in the 20–80 nm range. These findings corroborate the present study, highlighting the role of synthesis parameters and bioactive compounds in determining the structural characteristics of ZnO nanoparticles.

Energy dispersive analyses: Energy-dispersive X-ray (EDX) analysis was performed to determine the elemental composition of the green-synthesized ZnO nanoparticles (Fig. 6). The EDX spectrum, recorded over the 0–14 keV range, displayed strong signals corresponding to zinc and oxygen, confirming the successful formation of ZnO. The atomic composition was approximately 61% oxygen and 23% zinc. A notable carbon peak (~39%) was also detected, likely originating from phytochemicals present in the plant extract used during synthesis. These results suggest high elemental purity of ZnO NPs, with minimal contamination from extraneous elements. Elemental analysis through EDX is commonly used to verify the composition and purity of ZnO nanoparticles synthesized via green methods. Previous study of Yedurkar *et al*., (2016), EDX confirmed the presence of zinc and oxygen with no significant impurities, showing a composition of 77.56% zinc and 22.44% oxygen, indicating high-purity nanoparticle formation. Chikkanna *et al*., (2019) also reported prominent signals for zinc and oxygen, along with minor traces of elements such as carbon, calcium, silicon, and sulfur. These additional elements are likely introduced by plant-based compounds acting as natural stabilizers during synthesis. Nagarajan *et al*., (2013) noted well-defined peaks for zinc and oxygen, with the absence of other signals confirming nanoparticle purity. The present study shows comparable results, with EDX analysis demonstrating dominant zinc and oxygen peaks, validating the successful and clean biosynthesis of ZnO nanoparticles.

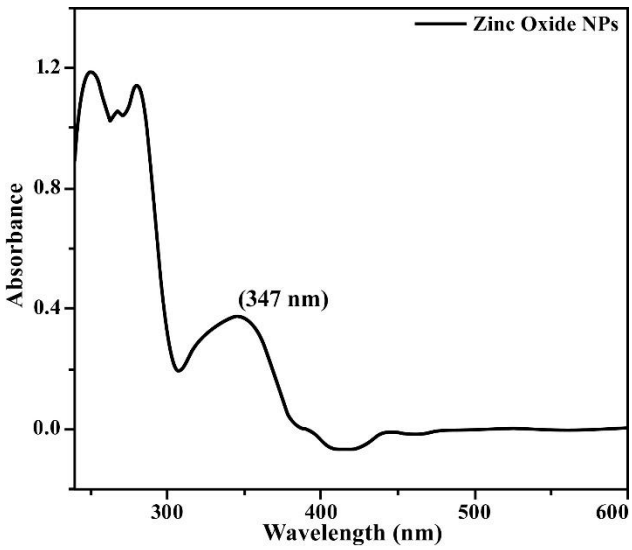

Fig. 2. UV spectrum of ZnONPs by using *Kalanchoe pinatta* leaf extract.

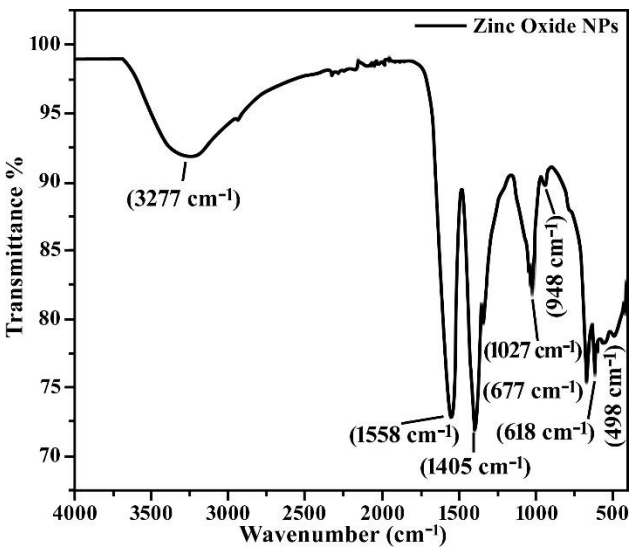

Fig. 3. FTIR spectrum of ZnONPs by using *Kalanchoe pinatta* leaf extract.

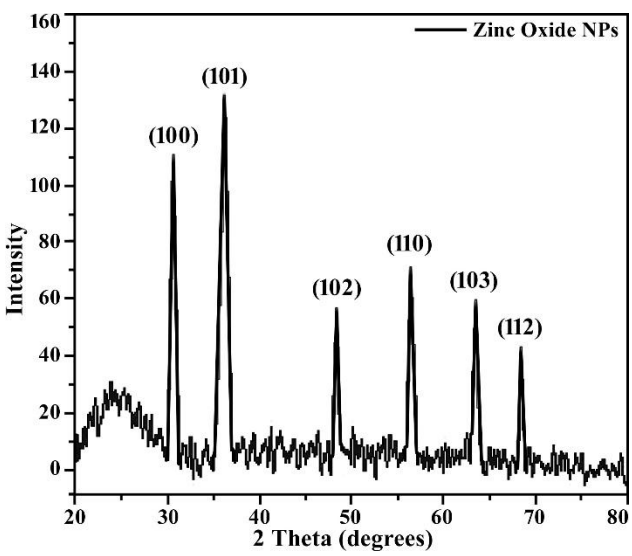

Fig. 4. XRD pattern of green-synthesized ZnO nanoparticles confirming crystalline structure and phase purity.

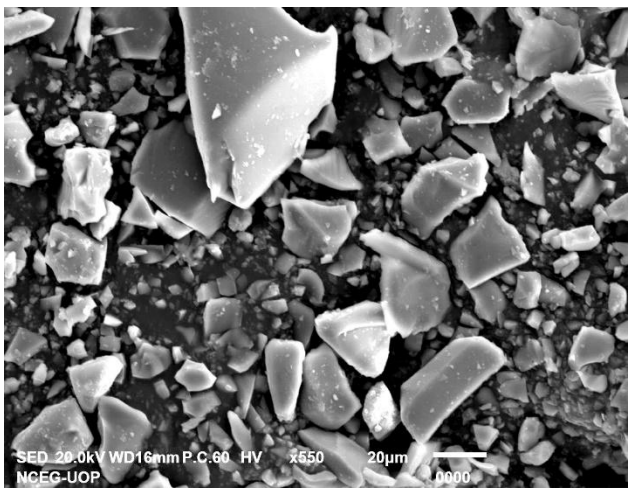

Fig. 5. SEM images of green-synthesized ZnO nanoparticles showing surface morphology and particle aggregation.

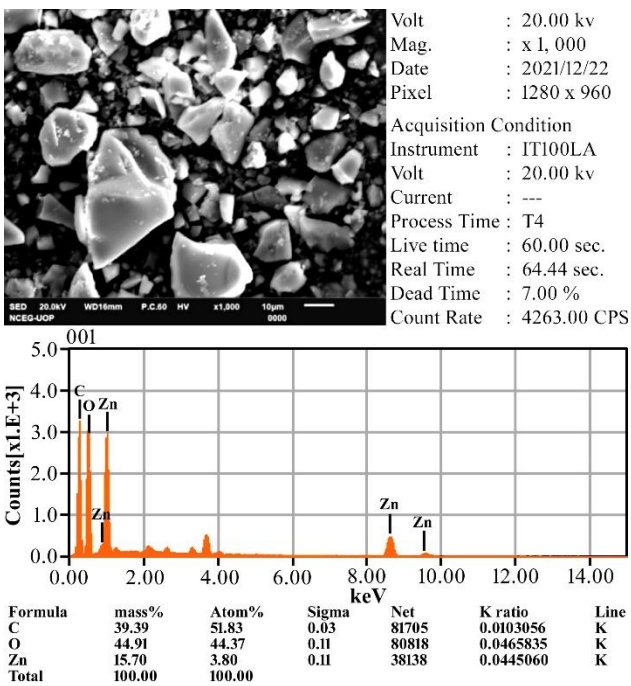

Fig. 6. EDX Graph of ZnONPs by using *Kalanchoe pinatta* leaf extract.

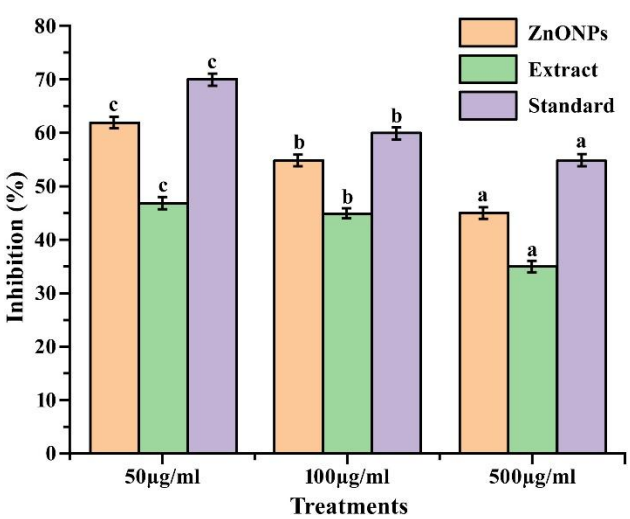

Fig. 7. Antioxidant activity of green-synthesized ZnO nanoparticles, plant extract, and ascorbic acid at different concentrations.

Biological assays

Antioxidant assay: The DPPH assay was conducted to assess the free radical scavenging ability of both the plant extract and the green-synthesized ZnO nanoparticles. The ZnONPs showed a concentration-dependent increase in antioxidant activity (Fig. 7). At concentrations of 50 µg/mL, 100 µg/mL, and 500 µg/mL, the scavenging effect increased steadily. The highest level of DPPH inhibition was recorded at 500 µg/mL, where ZnO nanoparticles achieved a 62.5% inhibition rate (p<0.0001), compared to 47.7% inhibition by the plant extract at the same concentration. The standard reference, ascorbic acid, exhibited the most significant effect, showing 70.3% inhibition at 500 µg/mL (p<0.0001). These results indicate that ZnONPs possess considerable antioxidant activity, likely enhanced through the green synthesis process.

It was suggested that Ag-NPs exhibited a significant (p<0.0001) maximum competency of DPPH radical inhibition, with the highest inhibition at 500µl/ml being 78.92%, and the least inhibition at 50µl/ml being 69.7% (Asad *et al.*, 2025a). Furthermore, *Grewia optiva* leaf extract demonstrated the highest inhibition at 500µl/ml being 75%, and the least inhibition at 50µl/ml being 65%, while ascorbic acid showed maximum significant (p<0.0001) inhibition at 77.4%.

Free radicals are known to cause oxidative damage to biological molecules, compromising cellular integrity and function. Vidhu *et al*., (2015) highlighted that biomolecules interacting with molecular oxygen can lead to the formation of reactive oxygen species, making antioxidants essential for maintaining cellular health by neutralizing these radicals. Suresh *et al*., (2015) demonstrated that the antioxidant capacity of ZnO nanoparticles synthesized using mango plant extract was comparable to that of vitamin C. Their DPPH scavenging assay, conducted in triplicate across various concentrations, confirmed that the green synthesis approach enhanced the radical scavenging potential of ZnONPs. These nanoparticles may exhibit even greater antioxidant activity if further engineered or functionalized. Similarly, Vera *et al*., (2023) reported that the type of plant extract significantly influenced the yield and antioxidant performance of the resulting ZnONPs. *Aristotelia chilensis* extract yielded the highest amount of ZnONPs, while *Galega officinalis* extract yielded the lowest. Extracts with high total phenolic content (TPC) were associated with increased antioxidant activity, suggesting that the phytochemical composition played a critical role in both nanoparticle synthesis and bioactivity. In ZnO nanoparticle production, extracts with greater antioxidant properties also demonstrated superior reducing and metal-chelating abilities, achieving scavenging efficiencies as high as 89.37%.

Antifungal activity: The antifungal efficacy of green-synthesized ZnO nanoparticles was evaluated against *Aspergillus niger* at concentrations of 50 µg/mL, 100 µg/mL, and 500 µg/mL, with clotrimazole used as a standard control. As shown in (Fig. 8), ZnONPs exhibited a concentration-dependent inhibitory effect, producing a significant (p<0.0001) zone of inhibition measuring 7.0 mm at 500 µg/mL, 5.5 mm at 100 µg/mL, and 4.5 mm at 50 µg/mL. In comparison, the plant extract alone showed inhibition zones of 6.0 mm at 500 µg/mL and 5.0 mm at 100 µg/mL. Interestingly, clotrimazole, despite being a standard antifungal

agent, showed a smaller inhibition zone of 4.5 mm at 500 µg/mL under the same conditions. These results suggest that ZnONPs synthesized via green methods possess notable antifungal activity, potentially exceeding that of conventional antifungal drugs at the tested concentration. Sun *et al*., (2018) reported that ZnO nanoparticles possessed significant antifungal activity, making them effective agents for managing fungal infections. Antifungal activity of ZnO nanoparticles has been extensively studied and supported by various findings. Asad *et al*., (2025a) demonstrated that plant leaf extract exhibited significant antifungal effects against *A. niger*, with inhibition zones of 4.9 mm and 4.4 mm at 500 µL/mL and 100 µL/mL, respectively ($p<0.05$). Clotrimazole, used as a reference antifungal agent, produced a smaller inhibition zone of 3.0 mm under similar conditions. Ag-NPs also displayed antifungal activity, with the highest inhibition zone recorded at 5.7 mm for 500 µL/mL, and 4.8 mm and 4.4 mm at 100 µL/mL and 50 µL/mL, respectively. Baskar *et al*., (2013) conducted diffusion assays against multiple fungal strains including *A. fumigatus*, *A. aculeatus*, and *A. niger*, and found that synthetic ZnONPs exhibited clear zones of inhibition on all test plates, indicating potent antifungal activity. This was attributed to the generation of highly reactive oxygen species (ROS) such as hydroxyl ions (OH^-), hydrogen peroxide (H_2O_2), and superoxide (O_2^{2-}), which are known to damage fungal cell walls and membranes.

Miri *et al*., (2019) further supported the antifungal potential of ZnONPs by demonstrating activity against *Candida albicans*, reporting minimum inhibitory concentration (MIC) and minimum biofilm suppression (MBS) values of 128 and 256 µg/mL, respectively. Their study suggested that ZnONPs compromised the integrity of fungal cell membranes, resulting in leakage of essential cellular components such as proteins, ions, and nucleic acids, ultimately leading to cell death.

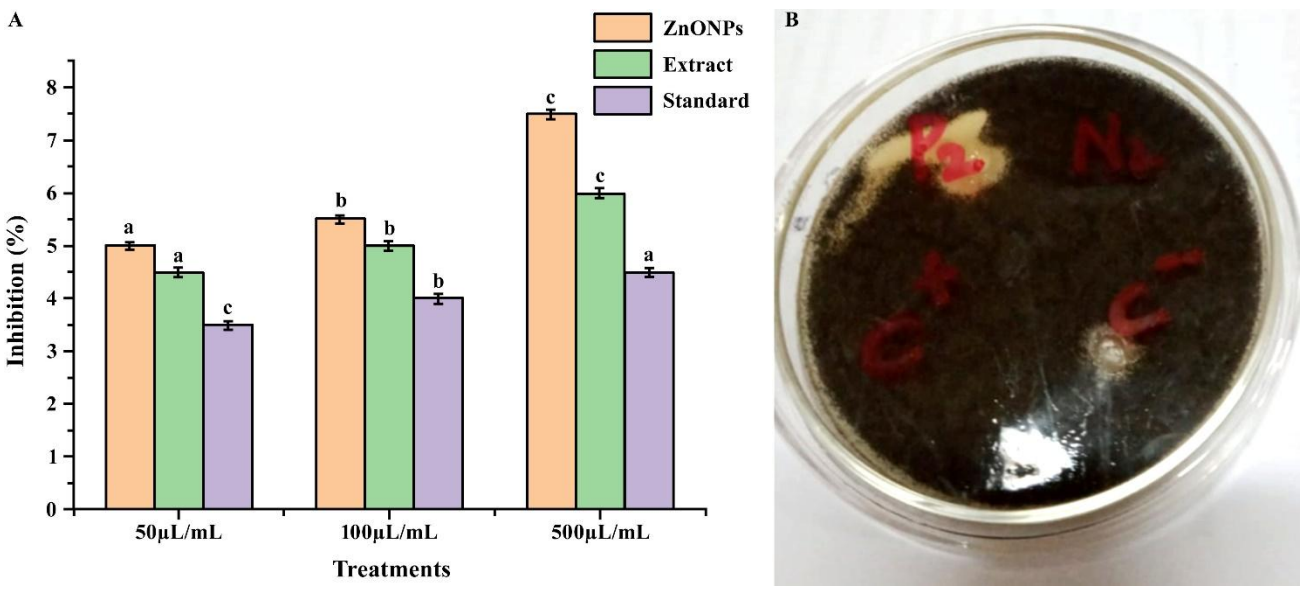

Fig. 8. (A) Antifungal activity of green-synthesized ZnO nanoparticles, plant extract, and clotrimazole against *Aspergillus niger* at different concentrations. (B) Representative image showing the inhibition zone of ZnO nanoparticles against *A. niger.*

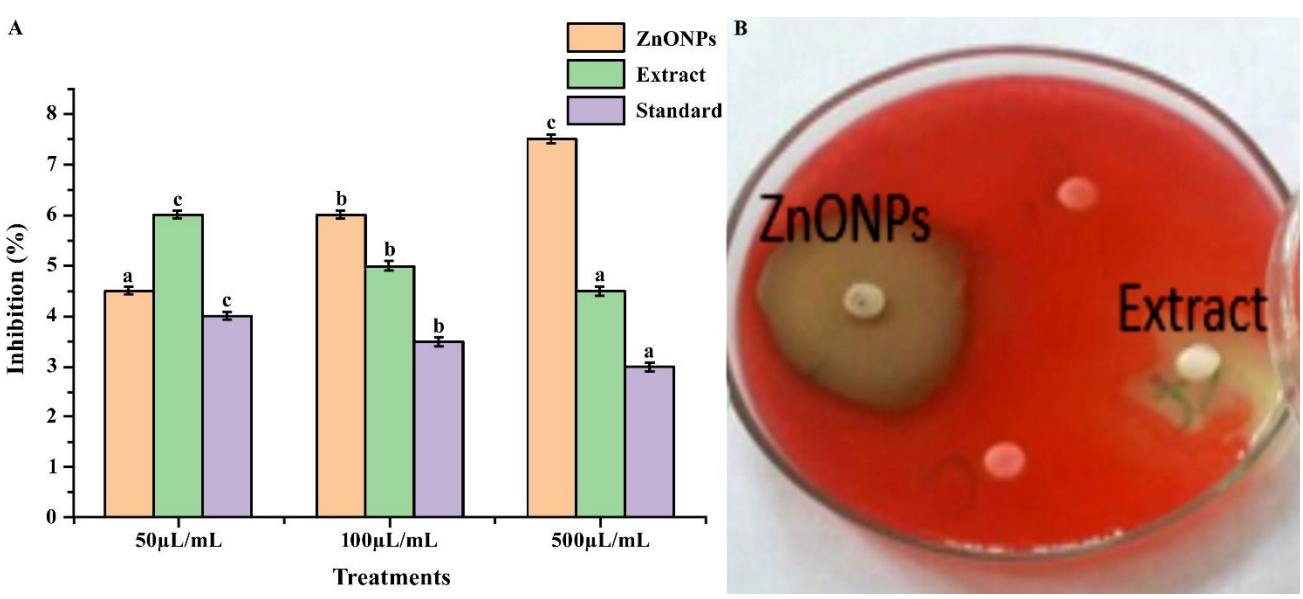

Fig. 9. (A) Antibacterial activity of green-synthesized ZnO nanoparticles at different concentrations against *Escherichia coli.* (B) Zone of inhibition observed in the antibacterial assay using *Kalanchoe pinnata* leaf extract and ZnO nanoparticles.

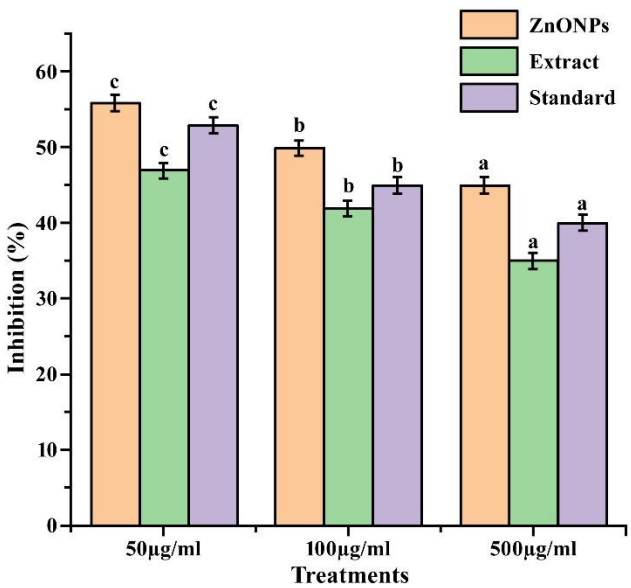

Fig. 10. Analgesic activity of green-synthesized ZnO nanoparticles at different concentrations compared to *Kalanchoe pinnata* leaf extract and standard drug (paracetamol), showing percentage inhibition of pain response.

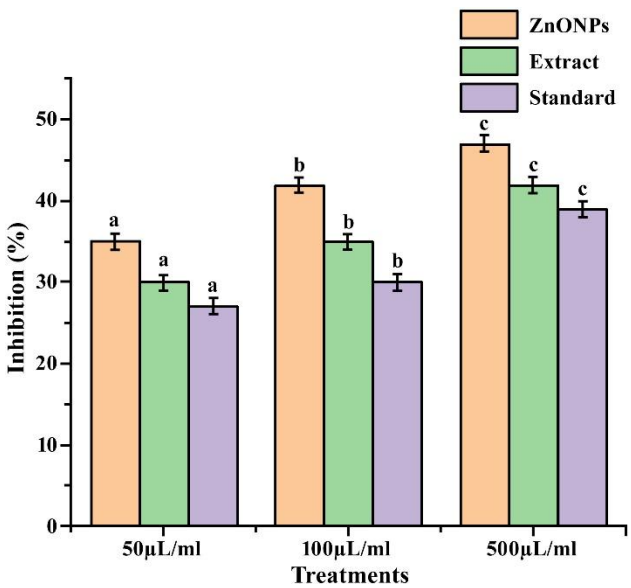

Fig. 11. Anti-inflammatory activity of green-synthesized ZnO nanoparticles at different concentrations, compared with *Kalanchoe pinnata* leaf extract and standard drug (diclofenac sodium), based on xylene-induced ear edema model in mice.

Table 1. Rectal temperature (°F) of albino mice before and after treatment with *Kalanchoe pinnata* leaf extract and ZnONPs in a Brewer's yeast-induced pyrexia model.

Group	Dose (µL/mL or mg/mL)	Baseline Temp. (°F)	0 h	1 h	2 h	3 h	4 h
Negative control (Saline)	10% v/v	98.7	101	101	101	101	101
Positive control Paracetamol)	1 mg/mL	98.7	100.5, 99.0, 100.0	100.1, 99.5, 99.0	100.1, 98.1, 99.4	100.6, 99.0, 98.2	100.3, 99.0, 98.0
Leaf extract	50, 100, 500 µL/mL	98.7	100.0, 99.5, 98.6	99.7, 99.5, 98.2	100.0, 98.0, 99.5	100.0, 99.5, 98.3	100.2, 99.1, 98.6
ZnO Nanoparticles	50, 100, 500 µL/mL	98.7	100.5, 99.0, 100.0	100.1, 99.5, 99.0	100.1, 98.1, 99.4	100.6, 99.0, 98.2	100.3, 99.0, 98.0

Antibacterial activity: The antibacterial potential of green-synthesized ZnO nanoparticles was assessed against *Escherichia coli* using the agar well diffusion method, with streptomycin serving as the standard control. As shown in (Fig. 9), ZnONPs exhibited a significant (p<0.0001) concentration-dependent antibacterial effect. The maximum zone of inhibition was recorded at 7.5 mm for 500 µL/mL, followed by 6.0 mm at 100 µL/mL and 4.5 mm at 50 µL/mL. In comparison, the plant extract alone produced zones of inhibition measuring 6.0 mm at 500 µL/mL and 4.5 mm at 100 µL/mL. Streptomycin, used as a reference antibiotic, showed a 4.5 mm inhibition zone at 500 µL/mL. These results suggested that ZnO nanoparticles synthesized via green methods possessed strong antibacterial properties, surpassing those of both the crude plant extract and the standard antibiotic under the tested conditions. Asad *et al*., (2025a) worked on the well diffusion method to assess the antibacterial potential of (*G. optiva*) leaves extract and Ag-NPs against *E. coli* and *shigella*. The results demonstrated that the extract at 500µl/ml showed a significant (p<0.05) highest zone of inhibition (4.7mm) against *E. coli* and a minimal zone of inhibition (3mm) against *shigella*. Ag-NPs showed a significantly (p<0.05) highest inhibition zone (5.9 mm) against *E. coli* at 500µl/ml and a lowest inhibition zone (4.7 mm) against *shigella* at 100µl/ml.

Rizwan *et al*., (2010) found that ZnONPs enhanced the growth inhibition and the ZnONPs concentration in the wells and discs. Concentrations of ZnONPs and the type of bacteria affected the size of the inhibition zone since it was larger with the cocci bacteria type than the gram-positive bacteria. Comparing the result with the control, cell growth inhibition by ZnONPs was notable here. Furthermore, the analysis confirmed that the gram-positive organisms *S. aureus* and *S. epidermidis* had similar results as the two-gram negative organisms *E. faecalis* and *E. coli*. Mendes *et al*., (2022) showed that ZnONPs had IC100 values of 0.6 mM for both strains of *P. aeruginosa* and *E. coli*, which ultimately reduced their growth. The calculated IC100 values were 0.8 and 1.0 mM for *B. subtilis* and *S. aureus*, respectively. Antimicrobial resistance is known to be provided by a thin layer of peptidoglycan that exists between two membranes in gram-negative bacteria.

Analgesic Assay: The analgesic potential of ZnO nanoparticles synthesized using *K. pinnata* leaf extract was evaluated through a dose-dependent study (Fig. 10). The assay was conducted in triplicate using three concentrations: 50 µg/mL, 100µg/mL, and 500 µg/mL. ZnONPs showed the highest significant inhibition of pain response at 500µg/mL, with a percent inhibition of 56% (p<0.0001). At 100µg/mL, ZnONPs exhibited 50% inhibition, while the crude leaf extract showed 47% and 42% inhibition at 500 µg/mL and 100 µg/mL, respectively. The standard analgesic, paracetamol, also showed a significant inhibition of 53% at 500µg/mL

(p<0.0001). These findings suggest that ZnONPs derived from *K. pinnata* may possess effective analgesic properties, comparable to or exceeding those of conventional drugs at higher concentrations. Asad *et al*., (2025b) investigated the analgesic properties of *G. optiva* leaf extract and iron nanoparticles (FeNPs), reporting a significant (p<0.0001) inhibition of pain at 500 µL/mL. The extract alone showed 62.5% inhibition at this concentration and 60% at 100 µL/mL. FeNPs demonstrated even greater effectiveness, with 63% inhibition at 500 µL/mL and 62% at 50 µL/mL. In comparison, the standard analgesic, paracetamol, showed 51.5% inhibition under the same conditions. Sulaiman *et al.*, (2022) evaluated the analgesic activity of zinc oxide-based nanomedicines formulated with etoricoxib and montelukast. Their findings revealed that the ZE6 formulation exhibited superior pain inhibition compared to both standard drugs and other nanoformulations, even at half the dosage, highlighting the enhanced efficacy of nanoscale drug delivery systems.

Asad *et al*., (2022) explored the analgesic potential of silver nanoparticles synthesized from *Amaryllis vittata* leaf and bulb extracts. The leaf-derived Ag-NPs achieved the highest inhibition (p<0.05), reducing writhing responses to 2.75 ± 0.75. Paracetamol, used as a standard (150 mg/kg), reduced writhing to 9 ± 3.0 with 76.77% inhibition (p<0.05). The ethanolic leaf extract also demonstrated significant analgesic activity, reducing writhing to 7.5 ± 1.19 and achieving 80.64% inhibition at 500 µg/mL.

Anti-inflammatory in vivo assay: The anti-inflammatory potential of green-synthesized ZnONPs was assessed using the xylene-induced ear edema model in mice (Fig. 11). ZnONPs were applied topically at 50, 100, and 500 µL/mL concentrations. At 500 µL/mL, ZnONPs showed the inhibition percent (47.16%) after 24 hours. At 50 µL/mL, inhibition reached 41% after 1 hour. The leaf extract showed 42% inhibition at 100 µL/mL. Diclofenac sodium (standard) showed 41.94% inhibition at 500 µL/mL. These results indicate that ZnONPs exhibit strong, dose-dependent anti-inflammatory activity, surpassing both the plant extract and standard drug. Sulaiman *et al*., (2022) reported that zinc oxide-based nanoformulations of etoricoxib and montelukast exhibited enhanced anti-inflammatory activity, with stronger inhibition observed during the second and third hours of treatment. Among the formulations, ZE6 exhibited the highest percentage of inhibition, outperforming the free drugs on a weight basis. Similarly, Rangeela *et al*., (2019) showed that ZnONPs synthesized using *Phyllanthus emblica* (amla) fruit possessed significant anti-inflammatory potential. Rajakumar *et al*., (2018) also reported that ZnONPs synthesized from *Andrographis paniculata* leaf extract exhibited strong biological activity, including antioxidant, anti-diabetic, and anti-inflammatory effects, suggesting their potential for applications in food, cosmetics, and pharmaceuticals.

Anti-pyretic assay: Albino mice were used to assess the antipyretic activity of *K. pinnata* leaf extract and ZnO nanoparticles using the Brewer's yeast-induced pyrexia model. Fever was induced by subcutaneous injection of Brewer's yeast (20 mL/kg body weight). ZnONPs and plant extract were administered at concentrations of 50, 100, and 500 µL/mL, as shown (Table 1). Rectal temperatures were recorded hourly for four hours using a lubricated thermometer. At the second hour, treatment groups received 500 µL/mL of either ZnONPs or the leaf extract to evaluate their temperature-lowering effects.

Asad *et al.*, (2025b) evaluated the antipyretic effects of *Grewia optiva* leaf extract and iron nanoparticles (FeNPs) in albino mice using the Brewer's yeast-induced pyrexia model. Mice were administered 20% Brewer's yeast (20 mL/kg body weight), and rectal temperatures were monitored hourly over a four-hour period. Administration of 500 µL/mL of FeNPs at the second hour significantly reduced body temperature, followed by the extract indicating effective pyrexia control.

Similarly, the antipyretic activity of zinc oxide-based etoricoxib and montelukast nanoformulations was assessed by Sulaiman *et al.,* (2022). Mice received 10% Brewer's yeast (mL/kg), and those exhibiting a temperature rise of ≥0.6°C after 18 hours were selected. Intraperitoneal doses of nanoformulations (ZE4, ZE5, and ZE6) effectively reduced fever within the first hour of administration, outperforming standard drugs. These findings support the superior antipyretic efficacy of nano-based formulations compared to their conventional counterparts.

Conclusion

This study demonstrated the successful green synthesis of zinc oxide nanoparticles (ZnONPs) using *Kalanchoe pinnata* leaf extract. The synthesized ZnONPs, with an average crystallite size of approximately 18 nm, were confirmed through UV-Vis, FTIR, SEM, EDX, and XRD analyses. The nanoparticles exhibited notable antioxidant, antimicrobial, analgesic, anti-inflammatory, and antipyretic activities. These results highlight the potential of *K. pinnata* mediated ZnONPs as an eco-friendly and effective candidate for biomedical applications.

Acknowledgements

The authors wish to thank Dr. Waliullah Khan and Dr. Dilawar Farhan Shams, Professor's at the Abdul Wali Khan University Mardan, for their research support.

References

Acay, H., M.F. Baran and A. Eren. 2019. Investigating antimicrobial activity of silver nanoparticles produced through green synthesis using leaf extract of common grape (*Vitis vinifera*). *Appl. Ecol. Environ. Res*., 17(2): 4539-4546.

Agarwal, H., S.V. Kumar and S. Rajeshkumar. 2017. A review on green synthesis of zinc oxide nanoparticles – an eco-friendly approach. *Resour. Eff. Technol*., 3(4): 406-413.

Ajmal, M.S., R. Muneer, A. Saeed, M. Tanveer and M.A. Saeed. 2024. Synergistic role of green-synthesized zinc oxide nanomaterials in biomedicine applications. *Chem. Select.,* 9(36): e202402517.

Anjum, S., R. Khadim, S.Z.A. Shah, A. Hamid, S.A. Jan, Z.K. Shinwari, N. Ahmad and A. Ghafoor. 2019. Biochemical characterization of geographically diverse *Mentha* species from Azad Jammu and Kashmir. *Fresen. Environ. Bull.*, 28(2A): 1336-1344.

Nkemzi, A.Q., K. Okaiyeto, O. Oyenihi, C.S. Opuwari, O.E. Ekpo and O.O. Oguntibeju. 2024. Antidiabetic, anti-inflammatory, antioxidant, and cytotoxicity potentials of green-synthesized zinc oxide nanoparticles using the aqueous extract of *Helichrysum cymosum*. *3 Biotech.*, 14(12): 1-17.

Al-Snafi, A.E. 2013. The chemical constituents and pharmacological effects of *Bryophyllum calycinum*: A review. *Int. J. Pharm. Sci*., 4: 171-176.

Asad, K., M.S. Khan, S. Asad, E. Ibáñez-Arancibia, P.R. De los Ríos-Escalante, F. Badshah, M.A. Ahmad Tariq and S.T. Shah. 2025a. Biological synthesis of silver nanoparticles; its characterization and therapeutic potential using *Grewia optiva* leaves extract. *Braz. J. Biol*., 85: e289190.

Asad, K., M.S. Khan, E. Ibáñez-Arancibia, P.R. De los Ríos-Escalante, F. Badshah, M.A. Ahmad and A. Khan. 2025b. Biological synthesis of iron nanoparticles: Characterization and therapeutic potential using *Grewia optiva* leaf extract. *Ital. J. Food Sci*., 37(2): 134-148.

Asad, K., S. Shams, E. Ibáñez-Arancibia, P.R. De los Ríos-Escalante, F. Badshah, F. Ahmad, M.S. Khan and A. Khan. 2024. Anti-inflammatory, antipyretic, and analgesic potential of chitin and chitosan derived from cockroaches (*Periplaneta americana*) and termites. *J. Funct. Biomater.*, 15(3): 80.

Asad, S., N. Anwar, M. Shah, Z. Anwar, M. Arif, M. Rauf, K. Ali, M. Shah, W. Murad, G.M. Albadrani and A.E. Altyar. 2022. Biological synthesis of silver nanoparticles by *Amaryllis vittata* (L.) Herit: From antimicrobial to biomedical applications. *Material*, 15: 5478.

Awwad, A. and M. Amer. 2020. Biosynthesis of copper oxide nanoparticles using Ailanthus altissima leaf extract and antibacterial activity. *Chem. Int.*, 7(1): 71-78.

Baskar, G., J. Chandhuru, K.S. Fahad and A.S. Praveen. 2013. Mycological synthesis, characterization and antifungal activity of zinc oxide nanoparticles. *Asian J. Pharm. Technol*., 3(4): 142-146.

Chemingui, H., T. Missaoui, J.C. Mzali, T. Yildiz, M. Konyar, M. Smiri, N. Saidi, A. Hafiane and H.C. Yatmaz. 2019. Facile green synthesis of zinc oxide nanoparticles (ZnO NPs): Antibacterial and photocatalytic activities. *Mater. Res. Express.*, 6(10): 1050b4.

Chikkanna, M.M., S.E. Neelagund and K.K. Rajashekarappa. 2019. Green synthesis of zinc oxide nanoparticles (ZnO NPs) and their biological activity. *SN Appl. Sci.*, 1(1): 117.

Das, S.N., J.P. Kar, J.H. Choi, T.I. Lee, K.J. Moon and J.M. Myoung. 2010. Fabrication and characterization of ZnO single nanowire-based hydrogen sensor. *J. Phys. Chem.*, 114: 1689-1693.

Dipankar, C. and S. Murugan. 2012. The green synthesis, characterization and evaluation of the biological activities of silver nanoparticles synthesized from *Iresine herbstii* leaf aqueous extracts. *Colloids Surf. B.*, 98: 112-119.

Golmohammadi, M., M. Honarmand and S. Ghanbari. 2020. A green approach to synthesis of ZnO nanoparticles using jujube fruit extract and their application in photocatalytic degradation of organic dyes. Spectrochim. *Acta A Mol. Biomol. Spectrosc.*, 229: 117961.

Iqbal, A., M. Mukherjee, J. Rashid, S.A. Khan, M.A. Ali and M. Arshad. 2019. Development of plant-microbe phytoremediation system for petroleum hydrocarbon degradation: An insight from alkB gene expression and phytotoxicity analysis. *Sci. Total Environ.,* 671: 696-704.

Jan, S.A., Z.K. Shinwari, M. Faizan and S. Ijaz. 2022. Anticancer properties of soybean: an updated review. *J. Cancer Prev. Curr. Res*., 13(1): 22-23.

Jiang, J., J. Pi and J. Cai. 2018. The advancing of zinc oxide nanoparticles for biomedical applications. *Bioinorg. Chem. Appl*., 2018(1): 1062562.

Keshari, A.K., R. Srivastava, P. Singh, V.B. Yadav and G. Nath. 2020. Antioxidant and antibacterial activity of silver nanoparticles synthesized by *Cestrum nocturnum*. *J. Ayurveda Integr. Med.*, 11: 37-44.

Khan, N., S. Fazal, R.M. Malik, S. Azam, A. Kanwal, Z.K. Shinwari, A.K. Shinwari and S.A. Jan. 2023. *In-silico* analysis of turmeric as an anti-inflammatory agent against ACE2 receptor. *Pak. J. Bot.*, 55(2): 763-778.

Khan, I., Z.K. Shinwari, N.B. Zahra, S.A. Jan, S. Shinwari and S. Najeebullah. 2019. DNA barcoding and molecular systematics of selected species of family Acanthaceae. *Pak. J. Bot.*, 52(1): 205-212.

Khan, N., A.P. Bano and P. Zandi. 2018. Effects of exogenously applied plant growth regulators in combination with PGPR on the physiology and root growth of chickpea (*Cicer arietinum*) and their role in drought tolerance. *J. Plant Interact.*, 13: 239-247.

Krupa, A.N.D. and R. Vimala. 2016. Evaluation of tetraethoxysilane (TEOS) sol–gel coatings, modified with green synthesized zinc oxide nanoparticles for combating microfouling. *Mater. Sci. Eng. C.,* 61: 728-735.

Kumar, S.S., P. Venkateswarlu, V.R. Rao and G.N. Rao. 2013. Synthesis, characterization and optical properties of zinc oxide nanoparticles. *Int. Nano Lett.*, 3: 1-6.

Liu, H., P. Kang, Y. Liu, Y. An, Y. Hu, X. Jin, X. Cao, Y. Qi, T. Ramesh and X. Wang. 2020. Zinc oxide nanoparticles synthesised from *Vernonia amygdalina* shows the anti-inflammatory and antinociceptive activities in the mice model. *Artif. Cells Nanomed. Biotechnol.*, 48: 1068-1078.

Mahmood, A., T. Munir, M. Fakhar-e-Alam, M. Atif, K. Shahzad, K.S. Alimgeer, T.N. Gia, H. Ahmad and S. Ahmad. 2022. Analyses of structural and electrical properties of aluminium doped ZnO-NPs by experimental and mathematical approaches. *J. King Saud Univ. Sci.*, 34(2): 101796.

Mendes, C.R., G. Dilarri, C.F. Forsan, V.D.M.R. Sapata, P.R.M. Lopes, P.B. de Moraes, R.N. Montagnolli, H. Ferreira and E.D. Bidoia. 2022. Antibacterial action and target mechanisms of zinc oxide nanoparticles against bacterial pathogens. *Sci. Rep*., 12(1): 2658.

Miri, A., N. Mahdinejad, O. Ebrahimy, M. Khatami and M. Sarani. 2019. Zinc oxide nanoparticles: biosynthesis, characterization, antifungal and cytotoxic activity. *Mater. Sci. Eng. C.*, 104: 109981.

Mofolo, M.J., P. Kadhila, K.C. Chinsembu, S. Mashele and M. Sekhoacha. 2020. Green synthesis of silver nanoparticles from extracts of *Pechuel-loeschea leubnitziae*: Their anti-proliferative activity against the U87 cell line. *Inorg. Nano-Met. Chem.*, 50: 949-955.

Nagarajan, S. and K.A. Kuppusamy. 2013. Extracellular synthesis of zinc oxide nanoparticle using seaweeds of Gulf of Mannar, India. *J. Nanobiotechnol.*, 11: 1-11.

Nazir, A., A. Akbar, H.B. Baghdadi, S. ur Rehman, E. Al-Abbad, M. Fatima, M. Iqbal, N. Tamam, N. Alwadai and M. Abbas. 2021. Zinc oxide nanoparticles fabrication using *Eriobotrya japonica* leaves extract: Photocatalytic performance and antibacterial activity evaluation. *Arab. J. Chem.*, 14(8): 103251.

Ovais, M., A.T. Khalil, S.A. Jan, M. Ayaz, I. Ullah, W. Shinwari and Z. K. Shinwari. 2019. Traditional Chinese medicine going global: opportunities for belt and road countries. *Proc. Pak. Acad. Sci*., 56(3 SI): 17-26.

Padalia, H. and S. Chanda. 2017. Characterization, antifungal and cytotoxic evaluation of green synthesized zinc oxide nanoparticles using *Ziziphus nummularia* leaf extract. *Artif. Cells Nanomed. Biotechnol.*, 45(8): 1751-1761.

Rajakumar, G., M. Thiruvengadam, G. Mydhili, T. Gomathi and I.M. Chung. 2018. Green approach for synthesis of zinc oxide nanoparticles from *Andrographis paniculata* leaf extract and evaluation of their antioxidant, anti-diabetic, and anti-inflammatory activities. *Bioproc. Biosyst. Eng.*, 41: 21-30.

Rajeshkumar, S., S.V. Kumar, A. Ramaiah, H. Agarwal, T. Lakshmi and S.M. Roopan. 2018. Biosynthesis of zinc oxide nanoparticles using *Mangifera indica* leaves and evaluation of their antioxidant and cytotoxic properties in lung cancer (A549) cells. *Enzyme Microb. Technol.*, 117: 91-95.

Rangeela, M., S. Rajeshkumar, T. Lakshmi and A. Roy. 2019. Anti-inflammatory activity of zinc oxide nanoparticles prepared using amla fruits. *Drug Invent. Today.*, 11: 2358.

Rao, U.S., G. Srinivas and T.P. Rao. 2015. Influence of precursors on morphology and spectroscopic properties of ZnO nanoparticles. *Proced. Mater. Sci.,* 10: 90-96.

Rizwan, W., Y.S. Kim, M. Amrita, S.I. Yoo and H.S. Shin. 2010. Formation of ZnO micro-flowers prepared via solution process and their antibacterial activity. *Nanoscale Res. Lett.,* 5: 1675-1681.

Shinwari Z.K., S.A. Jan, A.T. Khalil, A. Khan, M. Ali, M. Qaiser and N.B. Zahra. 2018. Identification and phylogenetic analysis of selected medicinal plant species from Pakistan: DNA barcoding approach. *Pak. J. Bot.*, 50(2): 553-560.

Sivasankarapillai, V.S., J. Jose, M.S. Shanavas, A. Marathakam, M.S. Uddin and B. Mathew. 2019. Silicon quantum dots: Promising theranostic probes for the future. *Curr. Drug Targets.*, 20: 1255-1263.

Subramaniam, H., S. Djearamane, *et al*. 2024. Potential of zinc oxide nanoparticles as an anticancer agent: A review. *J. Exp. Biol. Agric. Sci.*, 10(3): 494-501.

Sulaiman, S., S. Ahmad, S.S. Naz, S. Qaisar, S. Muhammad, R. Ullah, M.K. Al-Sadoon and A. Gulnaz. 2022. Synthesis of zinc oxide based etoricoxib and montelukast nano formulations and their evaluation through analgesic, anti-inflammatory, anti-pyretic and acute toxicity activities. *J. King Saud Univ. Sci*., 34: 101938.

Sun, Q., J. Li and T. Le. 2018. Zinc oxide nanoparticle as a novel class of antifungal agents: Current advances and future perspectives. *J. Agric. Food Chem*., 66(43): 11209-11220.

Suresh, D., P.C. Nethravathi, H. Rajanaika, H. Nagabhushana and S.C. Sharma. 2015. Green synthesis of multifunctional zinc oxide (ZnO) nanoparticles using *Cassia fistula* plant extract and their photodegradative, antioxidant and antibacterial activities. *Mater. Sci. Semicond. Process.*, 31: 446-454.

Swidan, M.M., F. Marzook and T.M. Sakr. 2024. pH-sensitive doxorubicin delivery using zinc oxide nanoparticles: *In vitro* and *In vivo* studies. *J. Mater. Chem*., 12(25): 6257-6274.

Vera, J., W. Herrera, E. Hermosilla, M. Díaz, J. Parada, A.B. Seabra, G. Tortella, H. Pesenti, G. Ciudad and O. Rubilar. 2023. Antioxidant activity as an indicator of the efficiency of plant extract-mediated synthesis of zinc oxide nanoparticles. *Antioxidants*, 12(4): 784.

Vidhu, V.K. and D. Philip. 2015. Biogenic synthesis of SnO_2 nanoparticles: Evaluation of antibacterial and antioxidant activities. *Spectrochim. Acta A Mol. Biomol. Spectrosc.*, 134: 372-379.

Vijayakumar, S., G. Vinoj, B. Malaikozhundan, S. Shanthi and B. Vaseeharan. 2015. Spectrochim. *Acta A Mol. Biomol. Spectrosc.,* 137: 886-891.

Yedurkar, S., C. Maurya and P. Mahanwar. 2016. Biosynthesis of zinc oxide nanoparticles using Ixora coccinea leaf extract-A green approach. *Open J. Synth. Theory Appl*., 5: 1-14.

Yousaf, I. 2024. The current and future perspectives of ZnO NPs in the treatment of diabetes mellitus. *arXiv,* 2409.04486.